Journal of Materials Chemistry C

Accepted Manuscript

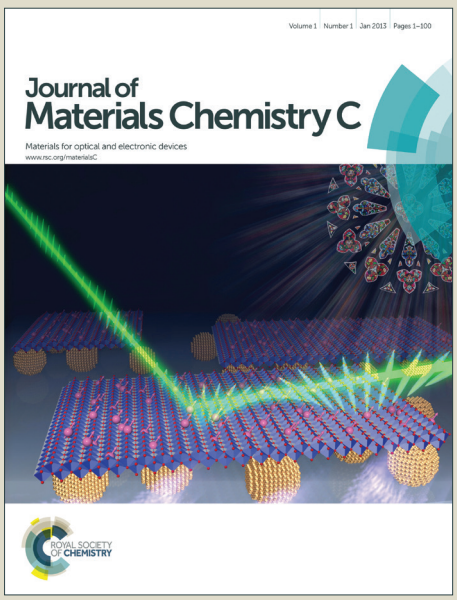

ROYAL SOCIETY OF CHEMISTRY

www.rsc.org/materialsC

Cite this: DOI: 10.1039/c0xx00000x

www.rsc.org/xxxxxx

ARTICLE TYPE

Fluorescence Property and Aggregation Behavior of Tetraphenylethene-Perylenebisimide Dyads

Yi Jia Wang,[a] Zeyu Li,[a] Jiaqi Tong,[a] Xiao Yuan Shen,[a] Anjun Qin[a,b], Jing Zhi Sun,[a,*] Ben Zhong Tang[a,b,c,*]

Received (in XXX, XXX) Xth XXXXXXXXX 20XX, Accepted Xth XXXXXXXXX 20XX

DOI: 10.1039/b000000x

Two tetraphenylethene (TPE) modified perylenebisimides (PBIs) were synthesized through linking the TPE moieties to PBI core at the imide positions. Theoretical calculations predict that, in both of the mono-TPE and di-TPE substituted derivatives (i. e. TPE-*N*-PBI and DTPE-*N*-PBI), the TPE and PBI units are orthogonal to each other, thus have no electronic conjugation. Thus the two compounds are TPE-PBI dyads rather than TPE-PBI conjugates. This property is supported by absorption and emission spectral features. In solution, aggregate and solid film, the fluorescence from both of TPE and PBI subunits are evidently quenched. The underlying mechanism is the photo-induced charge transfer between the electron donor TPE and electron acceptor PBI subunits. In high polar tetrahydrofuran/water mixture with large fraction of water, TPE-*N*-PBI can form *H*-aggregate. In low polar hydrophobic dichloromethane/hexane mixtures, due to the bulky size and rigidity of the TPE subunit, the dyad molecules cannot take a parallel alignment to form classical *J*- or *H*- aggregates, but have to exist a large offset angle. Consequently, X-aggregate is formed, which were confirmed by the absorption features, morphological observations and comparative investigation on reference compound.

1. Introduction

Perylenebisimide (PBI), a kind of organic dye with high optical and chemical stability, has attracted great research interest in the fields of *n*-type channel of organic field effect transistors,[1] synthetic light harvesting systems[2] and bio-/chemo-sensors.[3] Different structures and functions have been achieved by chemical modification with proper substitution at the imide positions and/or bay area of the PBI core. For example, modification at the imide positions by attaching perfluorocarbon chains afforded the PBI derivatives with high field effect charge mobility and stability, and the fabricated FETs could work in ambient condition.[4] By direct linking to conjugated units such as thiophenes and benzothiazoles at the bay positions, PBI-based dyes or conjugated polymers were derived, and the resultants showed improved performance in organic photovoltaic cells.[5] Highly fluorescent liquid crystals were obtained by attaching mesogens and bulky substituents at the imide and bay positions of PBI core, respectively.[6] The high emission efficiency of these liquid crystals benefited from the formation of *J*-aggregates in the solid state.

In addition to *J*-aggregation, the PBI-based dyads derived from chemical modification with tetraphenylethene (TPE) units at bay area of the PBI core demonstrated high fluorescence efficiency in solid states.[7] This observation is quite distinct from conventional PBI-based dyes, which are highly fluorescent in dilute solution but weakly emissive in aggregated states. This phenomenon refers to as aggregation-caused quenching (ACQ), which is due to the strong intermolecular interactions in molecular aggregates.[8] We associated the emission enhancement of the TPE-PBI dyads in solid state with the TPE units. TPE is a unique species of luminogen possessing aggregation-induced emission (AIE) instinct. AIE is the phenomenological description of a special emission property, for which the dyes are weakly or non-emissive in dilute solution but highly emissive in aggregate/solid states.[9] Direct attachment of TPE units at 1,6- or 1,7-positions of PBI core could turn the emission behavior of the PBI dyes from ACQ to AIE.[7a,c] Linking TPE units to the PBI core via oxygen atoms at 1,6- or 1,7-positions showed similar effect.[7b]

Considering that the chemical modification at imide positions is a widely used strategy to alter the solubility, molecular packing, self-assembling fashions, and photo/electronic properties, it is of scientific interest to examine the effects of the modification of PBI core with TPE units at the imide positions on the self-assembling behaviours and photophysical properties. To this end, we synthesized two TPE-PBI dyads, i.e. TPE-*N*-PBI and DTPE-*N*-PBI. As shown in Scheme 1, TPE-*N*-PBI is composed of one TPE and one PBI units; while DTPE-N-PBI contains two TPE and one PBI units. The two building blocks are directly linked by using the *N*-atoms as joints.

2. Experimental section

2.1 Materials and reagents.

3,4,9,10-Perylenetetracarboxylic dianhydride was purchased from Accelerating Scientific and Industrial Development thereby Serving Humanity. 2-Ethylhexylamine and 4-aminobenzophenone were purchased from Alfa Aesar and used as received without further purification. Other reagents including potassium

hydroxide, n-propanol, zinc acetate, imidazole, quinoline, benzophenone, zinc dust, titanium tetrachloride, pyridine, potassium carbonate, magnesium sulfate, ethyl acetate and dichloromethane (DCM) were purchased from Sinopharm Chemical Reagent Co., Ltd. Tetrahydrofuran (THF) was distilled under normal pressure from sodium benzophenone ketyl under nitrogen immediately prior to use.

2.2 Instrumentations.

^{1}H and ^{13}C NMR spectra were measured on a Mercury plus 300 MHz NMR spectrometer in $CDCl_3$ or *d*-DMSO with tetramethylsilane (TMS; $\delta = 0$ ppm) as internal standard. FT-IR spectra were recorded on a Bruker Vector 22 spectrometer as thin films on KBr pellets. High-resolution mass spectra (HRMS) were taken on a GCT premier CAB048 mass spectrometer operating in a MALDI-TOF mode. UV absorption spectra were taken on a Varian CARY 100 Bio spectrophotometer. Fluorescence (FL) spectra were recorded on a spectrofluorophotometer (RF−5301PC, SHIMADZU, Japan). Scanning electron microscope (SEM) images were taken on a JSM-5510 (JEOL, Japan) scanning electron microscope. Fluorescent images were taken with a Zeiss Axiovert 200 inverted microscope equipped with a 100 × oil immersion objective with a numerical aperture of 1.4 and an Ebq 100 Isolated electronic ballast for mercury vapor compressed-arc lamps. The fluorescence quantum efficiency (Φ_F) of the samples were estimated using fluorescein in ethanol (Φ_F = 70%) as standard. The absorbance of the solutions was kept between 0.04 and 0.06 to avoid the internal filter effect. Φ_F of the solid films were measured using integrating-sphere photometer.

2.3 Materials synthesis.

The synthetic routes towards the target compounds of M**1**, TPE-*N*-PBI and DTPE-*N*-PBI are shown in Scheme 1 and the detailed experimental procedures are described in the Electronic Supplementary Information (ESI). The reference compound M**1** was obtained by condensation reaction of the semi-hydrolyzed 3,4,9,10-perylenetetracarboxylic dianhydride (PTCDA) and 2-ethylhexylamine in H_2O-PrOH mixture at room temperature for 4 h and at 90 °C for another 2 h. The mono amino-functionalized tetraphenylethene (M**2**) was synthesized according to the procedures reported elsewhere.[10] By using zinc acetate as catalyst, condensation of M**1** and M**2** in imidazole solvent at elevated temperature (180 °C) afforded TPE-*N*-PBI in a yield of 24.1%. Reaction of PTCDA and M**2** at higher temperature (215 °C) in quinoline with the presence of $ZnAc_2$ resulted in DTPE-*N*-PBI. The yield was 44.2%. All of the compounds have been characterized with multiple spectroscopic technologies including ^{1}H NMR, ^{13}C NMR, FTIR, HRMS and the analytical data are satisfactory (see Figures S1 to S9 and the text in ESI for details).

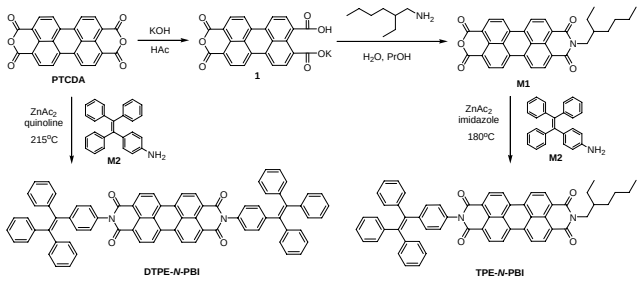

Scheme 1. Synthetic routes to tetraphenylethene-perylene bisimide dyads TPE-*N*-PBI and DTPE-*N*-PBI and the reference compound M**1**.

2.4. Theoretical Calculation.

All calculations on the considered molecules were performed by using the Gaussian 09 program package. B3lYP/6-31g (d) was employed to do the single point energy calculation based on the crystal structure. The relative energies of the HOMO and LUMO levels were obtained from the computed results.

The quenching factor Φ_q is calculated by using the equation of:

$\Phi_q = (\Phi_{solut} - \Phi_{aggre})/\Phi_{solut}$

Where Φ_{solut} and Φ_{aggre} are the emission quantum efficiency of the dye in dilute solution and in aggregation state, respectively.

3. Results and discussion

3.1. Aggregation models and their absorption and emission features

A PBI core can be viewed as an elliptical (discotic) chromophore. For this kind of chromophores, as illustrated in Fig. 1, their aggregation modes can be largely classified into four normal types. Based on this model, Types I and II exemplify two well-known close-packing modes, i.e. *H*- and *J*-aggregates, which can be determined when the angle θ between the chromophore's plane and the packing direction is more or less than a theoretical value of 54.7°, respectively.[11] According to exciton-coupling theory,[12] the absorption maximum splits into a strong blue-shifted peak and a relative weak red-shifted peak, and both peaks have reduced absorbance coefficient. While the fluorescence spectrum exhibits pronounced emission quenching and red-shifted peak. Type II or *J*-aggregate exhibits evidently red-shifted absorption spectrum and sharpened absorption peak. Meanwhile, its emission spectrum exhibits enhanced intensity and red-shifted peak. Type III is a special kind of *J*-aggregate, where the adjacent chromophores arrange with an offset angle (φ) between the long molecular axis. In this case, one dimensional column aggregation is expected to be formed. Type III aggregate displays the typical absorption and emission features of *J*-aggregate. Type IV is referred as to X-aggregate, where the angle φ is large enough to make transition dipole of the adjacent chromophores almost orthogonal to each other.[13] In this case, intermolecular electronic coupling is too weak to be obviously monitored. Consequently, both the absorption and emission spectra of the type IV aggregates display similar features to that of the isolated chromophore.

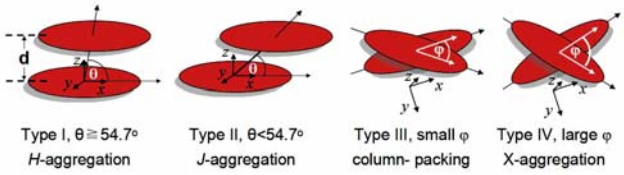

Figure 1. Illustration of aggregation modes of discotic chromophores. There are three key geometric parameters, d = the distance between two adjacent chromophores, θ = the tilted angle between the packing direction and the plane of the chromophore, and φ = the offset angle between the long molecular axes of the adjacent chromophores. The Cartesian coordinate system is shown to help understanding.

Organic chromophores can also form random aggregation, in which the chromophores are disorderly packed together. In this case, no long-range order can be achieved, but short-range order may exist in a certain degree. Thus, broadened and weakened absorption and emission features could be expected. There is also

a rare case that was observed for the PBI derivative with perfluorophenyl modifiers at the imide positions. The electron-withdrawing perfluorophenyl groups localized between the perylene cores thus isolated the π–π stacking.[14] This kind of aggregation can be ruled out here because the TPE groups cannot play the role as the perfluorophenyl groups do. All of the above-mentioned aggregates have their own spectral and morphological features. Our discussion will rely on the knowledge of the correlations between the aggregation types and the corresponding spectral and morphological features.

3.2. Electronic interaction between PBI and TPE units in isolated molecules

There are voluminous literature relating to substituted PBIs, and the substituents attached to the imide positions are mainly alkyls or alkyl/alkyloxyl modified phenyls, which have been used to improve the solubility and to tune the molecular packing. In single molecular level, these substitutions only have trivial influence on the electronic structure of the PBI core. Here, TPE is a conjugated unit and it has unique AIE property. TPE-*N*-PBI and DTPE-*N*-PBI can be considered as novel TPE-PBI dyads. It is important to examine whether the attachment of TPE at the imide positions of the PBI core has any electronic interactions with PBI core or not.

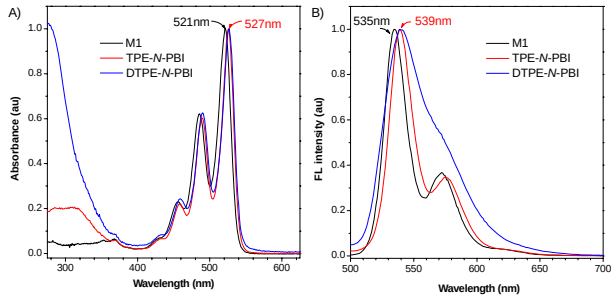

Figure 2. Absorption and fluorescence (FL) spectra of TPE-modified perylenebisimde dyads (TPE-*N*-PBI and DTPE-*N*-PBI) and the reference compound M**1**. Solvent: dichloromethane (DCM); Concentration of solutes: 10^{-5} M; Excitation wavelength: 480 nm.

To eliminate the latent interaction between aromatic solvent (e.g. toluene) and PBI/TPE unit, a hydrophobic (dichloromethane, DCM) and a hydrophilic (tetrahydrofuran, THF) solvents were used in the experiments. The UV-vis absorption spectra of TPE-*N*-PBI and DTPE-*N*-PBI dyes in their dilute DCM (10^{-5} M) solution were measured and the results are displayed in Fig. 2. For comparison, also shown in Fig. 2 is the UV-visible spectrum of M**1** in DCM solution (10^{-5} M). All three perylene-based dyes display very similar absorption features: the absorption bands cover between 400 and 550 nm, which are assigned to the S0–S1 transition of the PBI core with absorption maximum (λ_{abs}) and series of well-resolved vibronic structures that can be ascribed to the breathing vibration of the perylene skeleton.[15] For both TPE-*N*-PBI and DTPE-*N*-PBI, the λ_{max} appears at 527 nm, while for M**1** it appears at 521 nm. These molecules showed very similar absorption features in dilute THF solution (Fig. 4A and 5A). The spectral features observed above indicate that the TPE-substitution really has little influence on the electronic structure of the PBI core.

The above results are quite different from that observed for the PBI-dyes with substituents at bay positions. Due to steric repulsion, the bulky substituents at bay positions lead to core-twisted PBI-dyes. In comparison with the spectra of PBIs with substitutions only at the imide positions, the line-shape of the spectra for the bay-substituted dyes are broader and display less vibronic structures due to the loss of planarity of the perylene core and the lower molecular symmetry caused by the bay substituents.[6a, 15, 16] Recently, we found that the substitutions of TPE units at bay (1,6- or 1,7-) positions of PBI core resulted in the broadening of the absorption feature and the symmetrically forbidden S0–S2 transition band was evidently enhanced due to the core-twisting induced symmetry broken.

The fluorescence spectrum of TPE-*N*-PBI in DCM solution is shown in Fig. 2B, which is approximately the mirror image of its S0–S1 absorption bands. The emission peak appears at 539 nm with a pronounced shoulder at 575 nm. In dilute DCM solution, M**1** shows similar emission spectrum, with a peak and a shoulder at 535 and 572 nm, respectively (Fig. 2B). Such spectral features are typical for PBI derivatives with modification at the imide positions. Despite for the similarity of spectral features, the emission efficiency (Φ_F) of TPE-*N*-PBI and M**1** in DCM solution is dramatically different. When illuminated with UV light, TPE-*N*-PBI and M**1** emit dim and bright yellow-green light, respectively. By using fluorescein in ethanol (Φ_F = 70%) as the calibration, the Φ_F of TPE-*N*-PBI and M**1** in DCM solution is calculated to be 0.32% and 57.86% respectively, possessing a 180 times difference (ref. Fig. 4).

In accordance with our previous explanations to the fluorescence quenching of TPE-substituted PBIs at bay areas, the drastically reduced Φ_F of TPE-*N*-PBI can be tentatively associated with the intramolecular rotations of the phenyl groups of the TPE-unit, which largely exhaust the energy of the excited state. Another possible mechanism for the fluorescence quenching of TPE-*N*-PBI in dilute DCM solution is the process of energy transfer from TPE to PBI, which is frequently observed in the dyads constructed by two units having well-matched absorption and emission bands. As revealed by the absorption features, TPE and PBI units are individual parts and have only trivial electronic interaction in ground state. In photo-excited state, TPE emits greenish-blue fluorescence with emission peak at around 470-480 nm. This band falls into the S0–S1 transition absorption band of PBI, thus the fluorescent energy transfer from

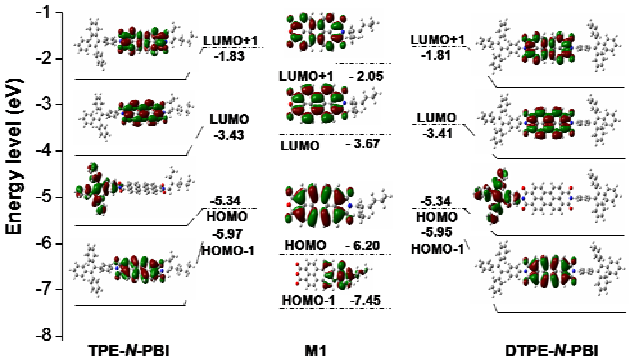

Figure 3. Diagram of the front orbitals energy level of TPE-*N*-PBI, DTPE-*N*-PBI and M**1**. HOMO and LUMO stand for the highest occupied molecular orbital and the lowest unoccupied molecular orbital.

TPE to PBI units is theoretically allowable. In fact, however, in dilute solution, the intramolecular rotations in TPE unit are active, thereby TPE unit is non-emissive. Consequently, the energy transfer process is an unimportant factor to the fluorescence quenching of TPE-*N*-PBI dyad. Moreover, when the TPE-*N*-PBI in dilute DCM solution was directly photo-excited by 480 nm light source, the solution was still faintly emissive. Therefore, the fluorescence quenching phenomenon cannot be addressed by the energy transfer mechanism.

Considering that PBI unit is a well-known electron acceptor (A) and TPE unit is an electron donor (D), electron transfer from TPE to PBI units at photo-excited state is a reasonable mechanism for the fluorescence quenching of TPE-*N*-PBI in dilute DCM solution. To verify this mechanism, we carried out theoretical calculations to TPE-*N*-PBI as well as its reference compounds DTPE-*N*-PBI and M**1**, and the data are shown in Fig. 3. It is found in the geometry of TPE-*N*-PBI that the plane of the phenyl group on TPE unit, which is directly linked to the PBI core via the *N*-atom, is nearly perpendicular to the plane of PBI core. As to the molecular orbital, TPE units have no electronic coupling with the PBI core. These results provide theoretical support to the experimental observations in absorption spectra.

In view of molecular orbital, TPE-*N*-PBI molecule takes the HOMO and LUMO orbitals from the HOMO of TPE and LUMO of PBI units, respectively. For DTPE-*N*-PBI, the HOMO is composed of the two degenerate HOMOs (on the same energy level) of the two TPE units. Identically to TPE-*N*-PBI, the LUMO of DTPE-*N*-PBI is the LUMO of PBI unit. The direct S0–S1 transition from the HOMO of TPE to the LUMO of PBI is a forbidden process in quantum mechanism, although calculation results assigned the HOMO and LUMO for TPE-*N*-PBI and DTPE-*N*-PBI. The vertical transitions from their own HOMOs to LUMOs are permitted processes. In fact, from 200 to 700 nm, PBI and TPE show their corresponding absorption bands with absorption maximum at 315 and 527 nm, respectively (Fig. 2A). The experimentally recorded absorption maxima are identical to that of TPE and PBI units, indicating that TPE and PBI separately play their absorption role but without electronic cross-talking. As the TPE unit is photo-excited, the electron on the LUMO of the TPE unit can transfer to the LUMO of PBI unit due to the energy level alignment. Based on the same principle, as the PBI unit is photo-excited, the electron on the HOMO of the TPE unit can transfer to the unoccupied HOMO of PBI unit (or hole on the HOMO of PBI transfer to the HOMO of TPE unit).

We explored further proofs by examining the electronic structure of TPE-*N*-PBI and M**1**. Cyclic voltammetry (CV) technique was used to determine the energy level of the molecules. It can be found that TPE-*N*-PBI shows a couple of reversible oxidation/reduction peaks under the negative bias. The reduction potential of TPE-*N*-PBI is approximate to most of the *N*-term substituted PBIs. This observation implies that the TPE substitution at the imide position leads little variation to the oxidation/reduction behaviors of PBI unit. By comparing the CV curve of TPE-*N*-PBI with that of M**1**, an excess oxidation peak an irreversible oxidation peak at around +0.85 V under the positive bias is observed. This signal is obviously associated with the TPE unit. Its appearance at positive bias indicates the electron donor character of TPE unit. The CV data reveal that linking a TPE donor at the imide position has no interference with the PBI core. The CV data of DTPE-*N*-PBI are unavailable due to its poor solubility in DCM and other organic solvents. The CV data suggest that, at least for the TPE-*N*-PBI dyad, the electron transfer process is one of the reasonable mechanisms of the observed fluorescence quenching in DCM solution.

All of the results, including the absorption and emission spectra, CV test, and theoretical calculation indicate that TPE and PBI units are individual components in the molecules of TPE-*N*-PBI and DTPE-*N*-PBI, although the TPE units are directly linked to PBI core at the imide positions. At ground state, there is no electronic coupling between TPE and PBI units, but at excited state the electron transfer from TPE to PBI unit is an energetically favourable process. Both active intramolecular rotation and electron transfer are the possible mechanisms to explain the drastic fluorescence quenching of TPE-*N*-PBI. More proofs are wanted to draw the final conclusion.

3.3. Absorption and emission of the dyads in DCM/hexane and THF/water mixtures

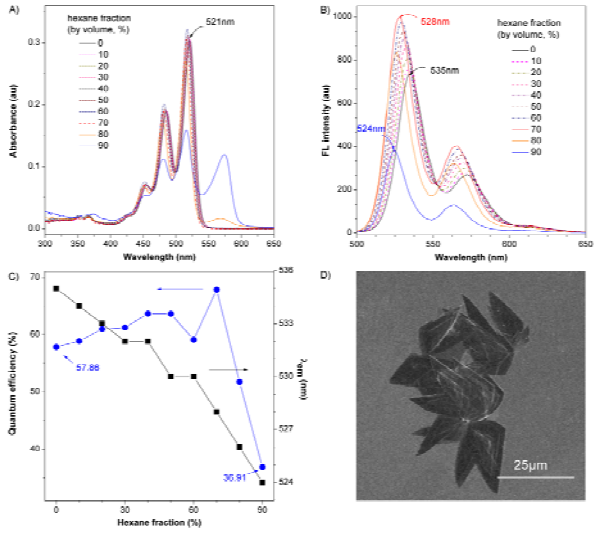

Figure 4. (A) Absorption and (B) FL spectra of M**1** in DCM/hexane mixtures with different hexane fractions (f_H). (C) The changes of the FL efficiency (Φ_F) and peak wavelength (λ_{em}) with f_H. (D) A typical image of the microstructure of M**1** in the DCM/hexane mixture with f_H of 90%.

As discussed in Section 3.1, different aggregation states have different spectral features, thus the aggregation behaviors of the PBI-TPE dyads can be investigated by monitoring the changes of the UV-vis spectral features in solution at different concentrations. Herein, we investigate the aggregation behaviors of TPE-*N*-PBI and DTPE-*N*-PBI dyads in the mixtures of two types of solvent/non-solvent mixtures. DCM and THF were used as solvents while hexane and water as non-solvents, which represent a hydrophobic and a hydrophilic system, respectively. At low concentration, aggregates can form when the fraction of non-solvent is high enough due to poor solubility of the dyes in the solvent and non-solvent mixture. This method is frequently used in monitoring the aggregate formation and fluorescence turn-on processes of AIE active molecules. For M**1**, in DCM/hexane system, the absorption spectra keep unchanged in line-shape when hexane fraction (f_H) changes from 0 to 70%. But at higher

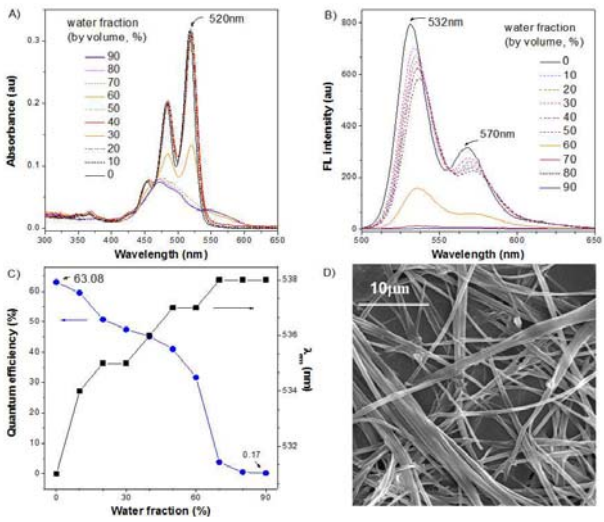

Figure 5. (A) Absorption and (B) FL spectra of M**1** in THF/water mixtures with different water fractions (f_W). (C) The changes Φ_F and λ_{em} with f_W. (D) A typical image of the microstructure formed by M**1** in the THF/water mixture with f_W of 90%.

f_H values (80 ~ 90%), the absorption feature undergoes dramatic changes. There appears a new peak with λ_{max} at around 575 nm, which is prominently red-shifted in comparison with the absorption peak in lower f_H. Meanwhile, the apparent absorption coefficient decreases evidently. These two signs indicate the strong electronic coupling between the perylene cores. Based on the understanding of the aggregation behavior of PBI-derivatives, the prominent red-shift is assigned to the formation of type I or face-to-face stacking aggregate.[15-17]

Similar behaviors have been observed for M**1** in THF/water mixtures, but the details have some differences (Fig. 5). Firstly, the threshold of dramatic absorption feature variation appears at the water fraction (f_W) of 60 %, which is lower than that observed for M**1** in DCM/hexane mixture (f_H = 70 %, Fig. 4). Secondly, at higher f_W values (80% ~ 90%), there appears a pronounced shoulder peaked at around 555 nm, which is prominently red-shifted in comparison with the absorption peak in lower f_H. Meanwhile, the main blue-shifted absorption peak appears at around 470 nm. Thirdly, the spectra greatly lost the fine structure at higher f_H values. The absorption spectra of the aggregated dyes agreed very well to those documents for the perylene bisimide pigments with alkyl substitutions at *N*-terms. For example, Graser and Hädicke reported similar absorption spectra of PBIs in the crystalline state.[18] These observations indicate the existence of strong intermolecular π–π interactions, and the formation of *H*-aggregate is expected. The observation of ordered micro-fibers is considered as a proof (Fig. 5D).

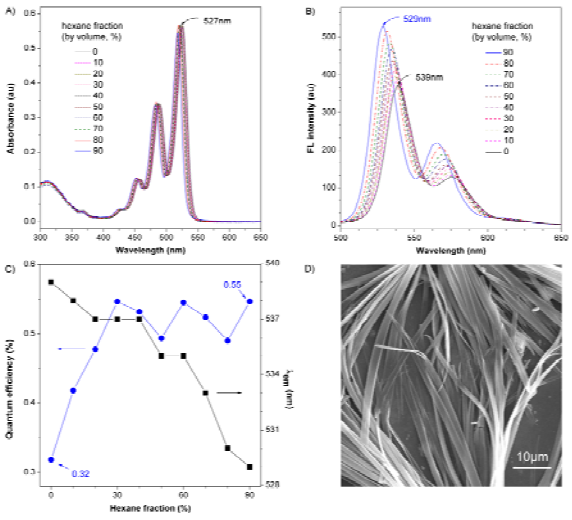

Figure 6. (A) Absorption and (B) FL spectra of TPE-*N*-PBI in DCM/hexane mixtures with different f_H values. (C) The changes of Φ_F and λ_{em} with f_H. (D) A typical image of the microstructure formed by TPE-*N*-PBI molecules in the DCM/hexane mixture with f_H of 90%.

For TPE-*N*-PBI in DCM/hexane mixtures, the absorption spectra are identical in line-shape and the absorption peak has no evident red- or blue-shift before f_H increases up to 90%. In general, the strong π–π stacking is the driving force of assembling process. The absence of the spectral signs of obvious blue- or red-shifted peaks and decreased coefficient in the absorption spectra implies that no strong π–π interaction exists between TPE-*N*-PBI molecules in the high f_H mixtures. Thus aggregation types I, II and III can be excluded from the possible aggregation states. Type IV is a possible aggregation state. Up to now, we can only draw a primary conclusion that that the modification with TPE at the imide positions of the PBI core has significant impacts on the aggregation behaviors of the TPE-modified PBI dyes.

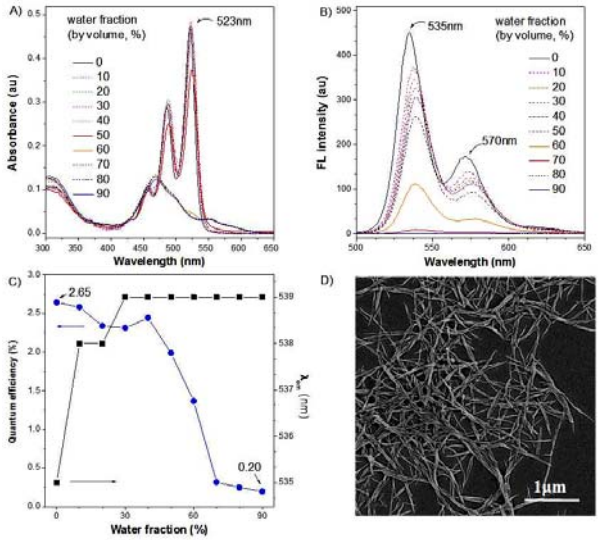

Figure 7. (A) Absorption and (B) FL spectra of TPE-*N*-PBI in THF/water mixtures with different f_W values. (C) The changes of Φ_F and λ_{em} with f_W. (D) A typical image of the microstructure formed by TPE-*N*-PBI molecules in the THF/water mixture with f_W of 90%.

In THF/water mixtures, the variation of the absorption features with f_w (Fig. 7A) looks like that observed for M**1** in THF/water mixtures (Fig. 5A). The maximal absorption peak shows evident blue-shift (523 nm to 470 nm) and a red-shifted (552 nm) when f_W is higher than 60%. As discussed above, such spectral line-shape indicates the presence of strong inter-chromophore π–π stacking and *H*-aggregate or Type-I aggregation is suggested to form. Up to now, we can only draw a primary conclusion that that the modification with TPE at the imide positions of the PBI core has significant impacts on the aggregation behaviors of the TPE-modified PBI dyes.

To get further understanding of the emission and aggregation

properties of TPE-*N*-PBI dyad, we measured the fluorescence spectra of TPE-*N*-PBI and its reference M**1** in DCM/hexane and THF/water mixtures with different f_H and f_W values. As shown in Fig. 4B, with the addition of hexane, the fluorescence spectra of M**1** show a monotonous and short blue-shift. When f_H changes from 0 to 60%, emission maximum (λ_{em}) undergoes blue-shift from 535 to 528 nm ($\Delta\lambda_{em}$ = 7 nm) and Φ_F increases from 57.86% to 67.89% ($\Delta\Phi_F$ = 10.03%). At higher f_H of 80% and 90%, Φ_F decreases quickly from 51.78% to 36.91%, respectively. Correlating these data with the absorption spectral data, it is found that, at f_H of 80% and 90%, M**1** molecules form face-to-face aggregate (Type-I) through strong π–π stacking, which induced the fluorescence quenching. In solid film, M1 has a low Φ_F = 0.9%. Consequently, M**1** is a typical fluorescent dye with aggregation-caused quenching (ACQ) property and the quenching factor (Φ_q) is calculated to be 36.3%. The observations of the spectral blue-shift and the small intensity enhancement in f_H range from 0 to 60% can be ascribed to the hydrophobic effect of the mixture solvent. With the increase of f_H, the dye molecules in the solvent localize in lower polar environment. According to the solvatochromic mechanism,[19] a polar chromophore exhibits shorter emission wavelength and higher emission efficiency in more hydrophobic solvents. M**1** is a low polar chromophore because of its symmetric conjugated skeleton.

The f_H related fluorescence spectra of TPE-*N*-PBI are shown in Fig. 6B. The λ_{em} shows monotonous blue-shift from 539 to 529 nm ($\Delta\lambda_{em}$ = 10 nm) when f_H increases from 0 to 90%. At the same time, the fluorescence intensity gradually increases, and Φ_F increases from 0.32% to 0.55%, equivalent to 72% emission enhancement. We ascribe the spectral blue-shift and the intensity enhancement to the weak solvatochromic effect in the mixture solvent, as described for the reference compound. A significant difference from the reference compound M**1** is that the emission intensity of TPE-*N*-PBI continues increasing when f_H increases from 80% to 90%; whereas M**1** begins to display its ACQ behaviour.

The emission behaviors of TPE-*N*-PBI in DCM/hexane mixtures with high f_H values imply that there is no strong electronic coupling or π–π interaction between the adjacent PBI cores. A simple linear extrapolation of the absorption and emission behaviours of the reference compound M**1** can lead to a conclusion that no aggregates of TPE-*N*-PBI molecules have been formed in the DCM/hexane mixtures with high f_H values. But this is not true because TPE-*N*-PBI has lower solubility in the DCM/hexane mixtures with high f_H values than M**1**. It is acceptable that the bulky size and the rigidity of the TPE moieties prevent TPE-*N*-PBI molecules from close packing in the aggregates. As discussed for absorption spectra, close packing modes of type I, II and III aggregations can be excluded in DCM/hexane mixtures. But the X-aggregate, or type IV is a possible being, because the weak intermolecular electronic coupling can only lead to small spectral variations.

In THF/water mixtures, however, the emission of M**1** shows different trend from that in DCM/hexane system (comparison Fig. 4 and Fig. 5). Due to the high polarity of aqueous environment, the emission spectra display a monotonous red-shift with addition of water (Fig. 5B and 5C). Meanwhile, the quantum efficiency exhibits continuously dropping from 63.08% to 0.17% at f_H = 0 and 90%, respectively, indicating that M**1** is a typical ACQ luminogen in THF/water solvent system. The Φ_q is calculated to be as high as 99.73%.

When we compare the emission behaviours of TPE-*N*-PBI in DCM/hexane and THF/water mixtures, it can be found that the dyad is weakly fluorescent in both systems, and Φ_F is measured to be 0.32% and 2.65%, respectively. But in the hydrophobic DCM/hexane mixture, the Φ_F increases with the addition of nono-polar hexane component; while in hydrophilic THF/water mixture, the Φ_F decreases with the addition of high polar water component. The oppositely shifted λ_{em} can be also found in these two systems. The changes of Φ_F are rationally associated with the variation of the environmental polarity and the shift of λ_{em} can be explained by the solvatochromic effect.

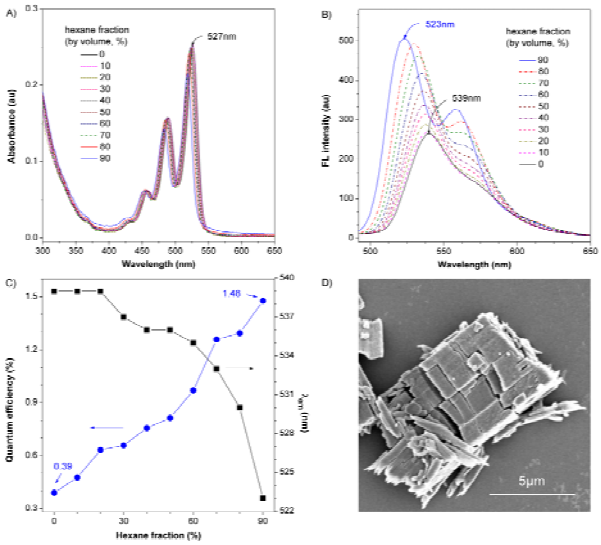

Figure 8. Absorption (A) and FL (B) spectra of DTPE-*N*-PBI in DCM/hexane mixtures with different f_H. (C) The changes of Φ_F and λ_{em} with f_H. (D) A typical image of the microstructure formed by DTPE-*N*-PBI in the DCM/hexane mixture with f_H of 90%.

The solubility of DTPE-*N*-PBI in THF is lower than 5 mg/L (< 10 μM), which is much less than in DCM. It is insoluble in water. As a result, we can only investigate its absorption and emission behaviours in DCM/hexane mixtures. As shown in Fig. 8A, the absorption spectra of this dyad show very small changes with the increase of f_H from 0 to 90%, which is similar to TPE-*N*-PBI. The emission behaviors of DTPE-*N*-PBI are also similar to TPE-*N*-PBI, but the enhancement of Φ_F shows a little difference. As displayed in Fig. 8C, the Φ_F of DTPE-*N*-PBI dyad increases from 0.39% to 1.48% when f_H changes from 0 to 90%. Meanwhile, λ_{em} blue-shifts from 539 to 523 nm ($\Delta\lambda_{em}$ = -16 nm). The higher fluorescence efficiency and larger intensity enhancement can be associated with the double TPE units in the DTPE-*N*-PBI dyad. The two TPE units strengthen the intramolecular D-A interaction, thereby lead to stronger solvatochromic effect. The spectral features of DTPE-*N*-PBI suggest that X-aggregate is a possible aggregation mode.

3.4. Morphology of the aggregates

So far, based on the absorption and emission spectra, we have inferred that TPE-*N*-PBI and DTPE-*N*-PBI dyads may take type-IV aggregation mode or X-aggregate in the low polar and

hydrophobic DCM/hexane mixtures, and TPE-*N*-PBI takes type-I or *H*-aggregate in the high polar and hydrophilic THF/water mixtures. It is a common phenomenon that the *H*-aggregate of PBIs tends to organize into ordered microstructures, because of the strong π-π interaction between the perylene cores. For TPE-PBI dyads, the bulky size and propeller shape of the TPE units may hinder the parallel packing of adjacent PBI cores and there should be an offset angle (φ) between the long molecular axis. Thus, an important issue is: what are effects of TPE moieties substituted at the imide positions on the morphology of TPE-PBI dyads?

To get direct information, we inspected the morphology of the aggregates with scanning electron microscope (SEM) technique. The typical images of the aggregates of the dyads TPE-*N*-PBI formed in the DCM/hexane and THF/water mixtures are displayed in Figures 6D and 7D, respectively. The non-solvent fraction of 90% for f_H and f_W was preferred owing to the evident aggregate formation of the dyad in this condition. In the mixture of DCM/hexane, bundles of microfibres are found in the field of microscope. The length of the fibers extends to several tens of micrometers. In THF/water mixture with f_W 90%, micro-fibers can be also observed in the SEM image, but the average size is smaller than that observed in DCM/hexane mixture. The size difference is associated with the fact that the highly hydrophobic dyad molecules have lower solubility in the polar hydrophilic environment; thus the aggregation takes place so quickly that aggregates cannot grow to larger size. The fibre-like morphology is usually observed for PBI derivative, including the PBI derivatives with TPE moieties at the bay positions,[7] which can be correlated to the preferentially one-dimensional molecular packing.

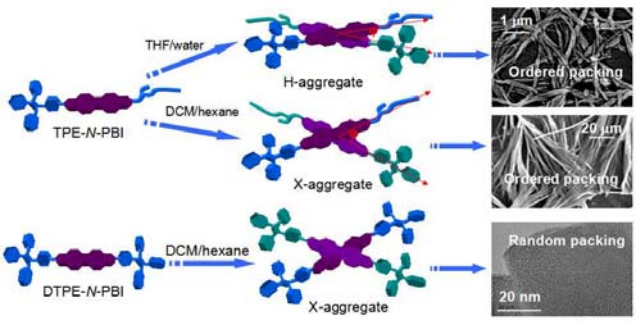

Figure 9. A schematic illustration of the aggregation of TPE-*N*-PBI and DTPE-*N*-PBI molecules in different situations. The pictures are the SEM images of TPE-*N*-PBI aggregates formed in THF/water (upper) and DCM/hexane (middle) mixtures and the high resolution TEM image of DTPE-*N*-PBI aggregate formed in DCM/hexane (bottom) mixtures.

The morphological observation implies that the π-π interaction between the perylene cores is still a strong driving force to organize the TPE-*N*-PBI molecules into ordered microstructures like that observed for its reference M**1** (Fig. 4D and 5D), despite the bulky size and propeller shape of the TPE unit at the one *N*-term. Correlating the morphological characters in image 6D and 7D with the absorption spectra in Fig. 6A and 7A, an obvious distinction is that the aggregation modes of TPE-*N*-PBI and DTPE-*N*-PBI molecules in the mixtures with high fraction of non-solvent are different. According to the solvation principle, in high polar THF/water mixtures, TPE-*N*-PBI molecules are highly polarized and tend to form *H*-aggregate that has a large θ and a smaller φ (Fig. 9). The repulsion barrier is partially overcome by the favorite static electrical attraction. While in low polar DCM/hexane mixture, TPE-*N*-PBI molecules are less polarized and take a X-shape aggregation to avoid the steric repulsion between the bulky TPE units.

For DTPE-*N*-PBI, the morphology of the aggregates is characterized by brick-like microstructures (Fig. 8D), which is distinct from those observed for TPE-*N*-PBI and M**1**. It seems that, in the aggregate of DTPE-*N*-PBI, the molecular packing has a three-dimensional characteristic. To get further information about the aggregate, high resolution transmittance electron microscope (HRTEM) measurement was carried out and the lattice image is shown as Fig. 9. The structure-less image indicates an amorphous character of the DTPE-*N*-PBI aggregate. It seems that the DTPE-*N*-PBI molecules randomly pack together. But this assumption is denied by the absorption spectra of DTPE-*N*-PBI in DCM/hexane mixtures, which suggest very weak intermolecular π-π interaction, because we have not recorded broadened and weakened absorption features corresponding to the existence of short-range order in random packing state. Furthermore, the diffraction patterns recorded from several selected sites of the aggregate display only dispersive halos without any recognizable array (Fig. S11). Accordingly, we propose a model as depicted in Fig. 9, the vertically adjacent DTPE-*N*-PBI molecules form X-aggregate due to the bulky volume of the two TPE units with a large off-set angle (φ). It has been reported that the C--H--π interaction between the phenyl groups plays key role in the formation of crystal and other kinds of ordered structures for many TPE derivatives.[20] But the C--H--π interaction in not strong enough thereby cannot extend to long range. Consequently, DTPE-*N*-PBI molecules cannot form large-sized 3-dimensional ordered structures, and the superficial brick-like structure (Fig. 8D) comes from random packing of the X-aggregate (Fig. 9).

3.5. Mechanism of the fluorescence quenching

It is noted that the emission behaviours of these two TPE-PBI dyads are quite different from that observed for PBI-derivatives with TPE substitutions at bay area (1,6- or 1,7- positions), which showed typical AIE behavior in DCM/hexane mixtures. The bay-substitutions interrupted the symmetric and planar conformation of the PBI core, and resulted in the absence of vibronic shoulder in the emission spectrum. In addition, TPE-substituents at the bay area are partially conjugated to the PBI core, thus resulted in pronouncedly red-shifted fluorescence emission. At the same time, their emission behaviors are different from the PBI-derivatives with alkyl-/alkyloxyl phenyl substitutions at imide positions, which show ACQ behavior or emission enhancement depending on the chemical structure of the substituents. For TPE-*N*-PBI and DTPE-*N*-PBI, the fluorescent emission is largely quenched in solution and aggregates. Therefore, the modification of PBI with TPE units at the imide positions has nontrivial influence on the optical properties of the resultants.

We measured the fluorescence spectra of the solid films cast from the solution of the dyads of TPE-*N*-PBI and DTPE-*N*-PBI. The results demonstrate that both of them are weakly emissive in solid film. Combing the fluorescent data of TPE-*N*-PBI and DTPE-*N*-PBI together, it is found that these two TPE-PBI dyads

are non- or faintly emissive in all cases including dilute solution, aggregates and solid films. Where has the fluorescence gone?

In the case of dilute solution, we have presented explanations to the fluorescence quenching in Section 3.2. We tentatively associated the observation with the intramolecular rotations of the phenyl groups of the TPE-units, which deplete the energy of the excited state. Now, based on the fluorescent behaviors of the two dyads in aggregation states, the mechanism of intramolecular rotations can be discarded. Because in aggregation states, the intramolecular rotations have been restricted, thus they cannot play the decisive role of energy-exhausting channel again. But in fact, the fluorescence of TPE-*N*-PBI and DTPE-*N*-PBI are still heavily quenched in the cases of aggregates and solid films. The quantum efficiency of both TPE-*N*-PBI and DTPE-*N*-PBI solid film is only 0.5%.

Formation of *H*-aggregate is another explanation to the fluorescence quenching phenomenon. This mechanism is plausible in the case of TPE-*N*-PBI in THF/water mixtures but fails in the explanation of the emission behaviours of TPE-*N*-PBI and DTPE-*N*-PBI in DCM/hexane mixtures. Absorption and emission spectral features, as well as SEM images provide sufficient proofs of the formation of X-aggregates. Therefore, another mechanism, or the photo-induced charge transfer is a more convincing mechanism for the fluorescence quenching of TPE-*N*-PBI and DTPE-*N*-PBI. The electronic process is depicted in Fig. 10.

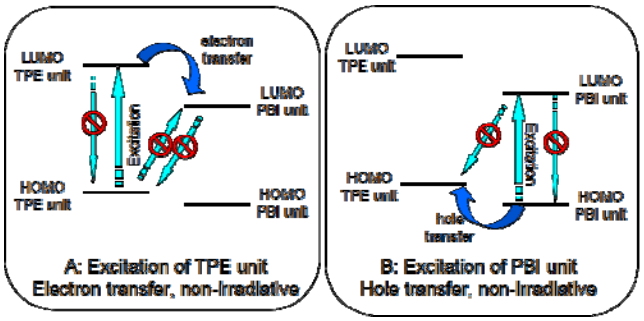

Figure 10. Mechanism of the overall fluorescence quenching behaviour of the TPE-PBI dyads with substitutions at imide positions. Processes A and B are corresponding to excitation on TPE and PBI units, respectively.

When a TPE unit is photo-excited, the photogenerated electron and hole localize in the LUMO and HOMO of TPE moiety. The transition from the HOMO of TPE to the LUMO of PBI is a forbidden process, though it is an energetically allowable process (cf. Fig. 3). The electron in the LUMO cannot recombine with the hole left in HOMO to give off fluorescence because the electron transfer from TPE's to PBI's LUMO is a predominated process, according to the ultrafast photoinduced charge transfer (PICT) mechanism.[21] Besides PICT, TPE is non-emissive in solution, according to the RIR mechanism of AIE phenomenon. Consequently, when TPE moiety is excited, the dyads are non-fluorescent in solutions; while in aggregates and in solid films, RIR process is achieved, the fluorescence quenching can be ascribed predominately to the PICT process. AIE takes a weak effect, which is reflected by the fact that the two dyads show higher fluorescent efficiency in aggregate than in solution (Fig. 6C and 8C).

When the PBI unit is photo-excited, the photogenerated electron and hole localize in the LUMO and HOMO of the central PBI moiety, due to the symmetric requirement of molecular orbital. The transition of the hot electron from the LUMO of PBI to the HOMO of TPE is a forbidden process. Meanwhile, the irradiative combination of the electron in the LUMO with the hole left in HOMO is process with very small probability because the PICT (the hole transfer from PBI's to TPE's HOMO) is a predominant process. Owing to the PICT, the dyads of TPE-*N*-PBI and DTPE-*N*-PBI are non-emissive in both solution and in solid/aggregate states.

The photo-induced intermolecular charge transfer process in PBI-based dyads was previously reported by Wasielewski and other groups.[2c, 2d, 22] For example, in a series of porphyrin-PBI dyads, when the PBI subunit in a dyad was excited under UV-light, it was proved that hole transport from the photo-excited PBI to the neutral porphyrin subunit is a dominant process that quenched the fluorescence of PBI. When the porphyrin subunit was excited, direct and efficient electron transfer from porphyrin (donor) to PBI (acceptor) occurred and the fluorescence of the porphyrin subunit was greatly quenched. In our present case, the porphyrin is replaced by TPE, which is not an electron donor as strong as porphyrin, but the photo-induced charge transfer process is still accessible according to their electronic structures. Fluorescence quenching in solution was also observed for PBI derivative substituted with trialkoxyphenyl groups at the imide positions.[16b, 18c] Würthner and co-workers ascribed the observed phenomenon to photo-induced electron transfer processes. Herein, the TPE is not only an electron donor, but also a special fluorogen that possesses AIE property. As a result, the dyads of TPE-*N*-PBI and DTPE-*N*-PBI bring something new forward to the PBI-based organic dyes.

Conclusions

We have demonstrated the effects of TPE-substitutions at the imide positions of PBI core on the absorption, emission and aggregation behaviors of the resultant TPE-PBI dyads. As a part of the sequence works, the properties of the dyads of TPE-*N*-PBI and DTPE-*N*-PBI are compared with their counterparts bearing TPE-substitutions at the bay positions of the PBI core. Due to the bulky size and rigidity of phenyl groups, TPE-*N*-PBI and DTPE-*N*-PBI molecules form *X*-aggregate in DCNM/hexane mixtures. Bearing a thinner alkyl chain, TPE-*N*-PBI molecules can form classical *H*-aggregate in THF/water mixtures when f_H is higher than 70%. In general, the PBI cores in X-aggregate emit strong fluorescence that is comparable to its solution, because of the weak dipole-dipole interaction between the adjacent PBI units. But it has been found that the both of TPE-*N*-PBI and DTPE-*N*-PBI are weakly emissive in dilute solution, microscopic aggregates and macroscopic solid films. This property is distinct from the AIE-active counterparts that have TPE-substitutions at the bay positions of PBI core. It is also distinct from the counterparts that have alkyl-/alkyloxy-phenyl substitutions at the imide positions, which normally show ACQ behaviour and sometimes show efficient emission both in solution and in aggregates. The "abnormal" fluorescent quenching behaviors are ascribed to the photo-induced electron transfer between TPE (D) and PBI (A) subunits, and this mechanism has been supported by the overall experimental data and the theoretically calculated

electronic structure of the dyads. In summary, TPE-substitutions at the imide positions of PBI core contributed new PBI derivatives, and they exhibit distinct optical properties and aggregation behaviors from a variety of TPE and PBI derivatives. These characteristics may help us, as the work is going on in our laboratory, to design novel TPE-PBI dyads and find applications in optical limiting materials and efficient charge transfer arrays.

Acknowledgement

This work was partially supported by the National Basic Research Program of China (973 program; 2013CB834704) and the National Science Foundation of China (51273175); the Research Grants Council of Hong Kong (16301614, N_HKUST 604/14, N_HKUST 620/11), the Innovation and Technology Commission (ICTPD/17-9) and the University Grants Committee of Hong Kong (AoE/P-03/08). J. Z. Sun thanks the support of the Open Project of State Key Laboratory of Supramolecular Structure and Materials (sklssm201322).

Notes and references

[a] *MoE Key Laboratory of Macromolecule Synthesis and Functionalization, Department of Polymer Science and Engineering, Zhejiang University, Hangzhou 310027, China. Fax: +86 571 87953734; Tel: +86 571 87953734;E-mail: sunjz@zju.edu.cn.*

[b] *Guangdong Innovative Research Team, State Key Laboratory of Luminescent Materials and Devices, South China University of Technology, Guangzhou 510640, China.*

[c] *Department of Chemistry, Institute for Advanced Study, State Key Laboratory of Molecular NeuroScience, and Division of Biomedical Engineering, The Hong Kong University of Science & Technology, Clear Water Bay, Kowloon, Hong Kong, China. Fax: +852-23581594; Tel: +852-23587375; E-mail: tangbenz@ust.hk*

† Electronic Supplementary Information (ESI) available: [The characterization data of M**1**, TPE-*N*-PBI and DTPE-*N*-PBI, including ^{1}H NMR, ^{13}C NMR, FTIR, MALDI-TOF mass spectra, cyclic voltammogram diagrams, and a summary of the optical and electromnic properties]. See DOI: 10.1039/b000000x/

1 (a) B. A. Jones, A. Facchetti, M. R. Wasielewski, and T. J. Marks, *J. Am. Chem. Soc*., 2007, **129**, 15259; (b) B. A. Jones, A. Facchetti, M. R. Wasielewski and T. J. Marks, *Adv. Funct. Mater.*, 2008, **18**, 1329; (c) R. Schmidt, J. H. Oh, Y. S. Sun, M. Deppisch, A. M. Krause, K Radacki, H. Braunschweig, M. Könemann, P. Erk, Z. Bao and F. Würthner, *J. Am. Chem. Soc.*, 2009, **131**, 6215; (d) S. Fabiano, S. Braun, M. Fahlman, X. Crispin, M. Berggren, *Adv. Funct. Mater.*, 2014, **24**, 695.

2 (a) A. P. H. J. Schenning, J. Herrikhuyzen, P. Jonkheijm, Z. Chen, F. Würthner and E. W. Meijer, *J. Am. Chem. Soc.*, 2002, **124**, 10252; (b) B. Rybtchinski, L. E. Sinks, M. R. Wasielewski, *J. Am. Chem. Soc*., 2004, **126**, 12268; (c) M. R. Wasielewski, *Acc. Chem. Res*., 2009, **42**, 1910; (d) V. V. Roznyatovskiy, R. Carmieli, S. M. Dyar, K. E. Brown, M. R. Wasielewski, *Angew. Chem. Int. Ed.*, 2014, **53**, 3457.

3 (a) X. Zhang, S. Rehm, M. M. Safont-Sempere and F. Würthner, *Nat. Chem.*, 2009, **1**, 623; (b) Y. Liu, K. R. Wang, D. S. Guo and B. P. Jiang, *Adv. Funct. Mater.*, 2009, **19**, 2230; (c) L. Wang, L. Xu, K. G. Neoh and E. T. Kang, *J. Mater. Chem.*, 2011, **21**, 6502; (d) T. Takada, A. Ashida, M. Nakamura, M. Fujitsuka, T. Majima, and K. Yamana, *J. Am. Chem. Soc.*, 2014, **136**, 6814.

4 (a) B. A. Jones, M. J. Ahrens, M. Yoon, A. Facchetti, T. J. Marks and M. R. Wasielewski, *Angew. Chem., Int. Ed.*, 2004, **43**, 6363; (b) H. Z. Chen, M. M. Ling, X. Mo, M. M. Shi, M. Wang and Z. Bao, *Chem. Mater.*, 2007, **19**, 816.

5 (a) C.-W. Ge, C.-Y. Mei, J. Ling, J.-T. Wang, F.-G. Zhao, L. Liang, H.-J. Li, Y.-S. Xie and W.-S. Li, *J. Polym. Sci. Part A-Polym. Chem.*, 2014, **52**, 1200; (b) X. Zhang, Z. Lu, L. Ye, C. Zhan, J. Hou, S. Zhang, B. Jiang, Y. Zhao, J. Huang, S. Zhang, Y. Liu, Q. Shi, Y. Liu and J. Yao, *Adv. Mater.*, 2013, **25**, 5791; (c) Y. Zhou, Q. Yan, Y.-Q. Zheng, J.-Y. Wang, D. Zhao and J. Pei, *J. Mater. Chem. A* 2013, **1**, 6609; (d) Y. Lin, Y. F. Li and X. W. Zhan, *Chem. Soc. Rev.*, 2012, **41**, 4245; (e) X. W. Zhan, A. Facchetti, S. Barlow, T. J. Marks, M. A. Ratner, M. R. Wasielewski and S. R. Marder, *Adv. Mater.*, 2011, **23**, 268.

6 (a) Z. Tian, A. D. Shallerz and A. D. Q. Li, *Chem. Commun.*, 2009, 180; (b) X.-Q. Li, X. Zhang, S. Ghosh and F. Würthner, *Chem. Eur. J.*, 2008, **14**, 8074; (c) H. Yoo, H. W. Bahng, M. R. Wasielewski and D. Kim, *Phys. Chem. Chem. Phys.*, 2012, **14**, 2001.

7 (a) Q. Zhao, S. Zhang, Y. Liu, J. Mei, S. Chen, P. Lu, A. Qin, Y. Ma, J. Z. Sun and B. Z. Tang, *J. Mater. Chem*., 2012, **22**, 7387; (b) Q. Zhao, K. Li, S. Chen, A. Qin, D. Ding, S. Zhang, Y. Liu, B. Liu, J. Z. Sun and B. Z. Tang, *J. Mater. Chem*., 2012, **22**, 15128; (c) Q. Zhao, X. A Zhang, Q. Wei, J. Wang, X. Y. Shen, A. Qin, J. Z. Sun and B. Z. Tang, *Chem. Commun*., 2012, **48**, 11671.

8 (a) J. B. Birks, *Photophysics of Aromatic Molecules*, Wiley, London, 1970; (b) S. W. Thomas III, G. D. Joly and T. M. Swager, *Chem. Rev.*, 2007, **107**, 1339; (c) X. Zhang, D. Gorl, V. Stepanenko and F. Würthner, *Angew. Chem. Int. Ed.*, 2014, **53**, 1070.

9 (a) Y. N. Hong, J. W. Y. Lam and B. Z. Tang, *Chem. Commun.*, 2009, 4332; (b) Y. N. Hong, J. W. Y. Lam and B. Z. Tang, *Chem. Soc. Rev.*, 2011, **40**, 5361; (c) J. Mei, Y. Hong, J. W. Y. Lam, A. Qin, Y. Tang and B. Z. Tang, *Adv. Mater.*, 2014, **26**, 5429.

10 X. Yang, X. Xu and H. F. Ji, *J. Phys. Chem. B* 2008, **112**, 7196.

11 (a) E. E. Jelly, *Nature*, 1936, **138**, 1009; (b) T. Kobayashi, *J-Aggregates*, Vol. 2, World Scientific, Singapore, 2012.

12 (a) E. G. McRae and M. Kasha, *J. Chem. Phys.*, 1958, **28**, 721; (b) M. Kasha, *Radiation Research*, 1963, **20**, 55.

13 (a) F. Steuber, J. Staudigel, M. Stössel, J. Simmerer, A. Winnacker, H. Spreitzer, F. Weissörtel and J. Salbeck, *Adv. Mater*., 2000, **12**, 130; (b) J. Cornil, D. Beljonne, J.-P. Calbert and J.-L. Bredas, *Adv. Mater.*, 2001, **13**, 1053; (c) X.-T. Chen, Y. Xiang, P.-S. Song, R.-R. Wei, Z.-J. Zhou, K. Li and A. J. Tong, *J. Lumin.*, 2011, **131**, 1453; (d) X. D. Zhang, J. W. Ye, L. F. Xu, L. J. Yang, D. Deng and G. L. Ning, *J. Lumin.*, 2013, **139**, 28.

14 (a) M. M. Shi, H. Z. Chen, J. Z. Sun, J. Ye and M. Wang, *Chin. Chem. Lett.*, 2004, **15**, 575; (b) M. M. Shi, H. Z. Chen, J. Z. Sun, J. Ye and M. Wang, *Chem. J. Chinese Univ.*, 2004, **25**, 454.

15 (a) M. Sadrai, L. Hadel, R. R. Sauers, S. Husain, K. Krogh-Jespersen, J. D. Westbrook and G. R. Bird, *J. Phys. Chem*., 1992, **96**, 7988; (b) Z. Chen, V. Stepanenko, V. Dehm, P. Prins, L. D. A. Siebbeles, J. Seibt, P. Marquetand, V. Engel and F. Würthner, *Chem. Eur. J.*, 2007, **13**, 436.

16 (a) R. Gvishi, R. Reisfeld, Z. Burshtein, *Chem. Phys. Lett.*, 1993, **213**, 338; (b) Z. Chen, U. Baumeister, C. Tschierske and F. Würthner, *Chem. Eur. J.*, 2007, **13**, 450.

17 (a) A. R. B. Martin, *Chem. Rev.*, 1996, **96**, 3043; (b) N. J. Baxter, M. P. Williamson, T. H. Lilley and E. Haslan, *J. Chem. Soc. Faraday Trans.2* 1996, **92**, 231; (c) P. van der Schoot, M. A. J. Michels, L. Brunsveld, R. P. Sijbesma and A. Ramzi, *Langmuir*, 2000, **16**, 10076.

18 a) E. Hädicke, F. Graser, *Acta Crystallogr. Sect. C* 1986, **42**, 189; b) G. Klebe, F. Graser, E. Hädicke, J. Berndt, *Acta Crystallogr. Sect. B* 1989, **45**, 69; c) F. Würthner, C. Thalacker, S. Diele and C. Tschierske, *Chem. Eur. J.*, 2001, **7**, 2245.

19 C. Reichardt, *Chem. Rev.*, 1994, **94**, 2319.

20 (a) H. Tong, Y. Q. Dong, Y. N. Hong, M. Häußler, J. W. Y. Lam, H. H. Y. Sung, X. M. Yu, J. X. Sun, I. D. Williams, H. S. Kwok, B. Z. Tang, *J. Phys. Chem. C*, 2007, **111**, 2287; (b) Z. Zhao, J. W. Y. Lam, B. Z. Tang, *J. Mater. Chem.*, 2012, **22**, 23726; (c) J. Q. Shi, N. Chang, C. H. Li, J. Mei, C. M. Deng, X. L. Luo, Z. P. Liu, Z. S. Bo, Y. Q. Dong, B. Z. Tang, *Chem. Commun*., 2012, **48**, 10675.

21 (a) G. Yu, J. Gao, J. C. Hummelen, F. Wudl and A. J. Heeger, *Science*, 1995, **270**, 1789; (b) J. J. M. Halls, C. A. Walsh, N. C. Greenham, E. A. Marselia, R. H. Friend, S. C. Moratti and A. B. Holmes, *Nature*, 1995, **376**, 498.

22 (a) M. P. O'neil, M. P. Niemczyk, W. A. Svec, D. Gosztola, G. L. Gaines III and M. R. Wasielewski, *Science*, 1992, **257**, 63; (b) T. Boom, R. T. Hayes, Y. Zhao, P. J. Bushard, E. A. Weiss and M. R. Wasielewski, *J. Am. Chem. Soc.,* 2002, **124**, 9582; (c) S. M. M. Conron, L. E. Shoer, A. L. Smeigh, A. B. Ricks and M. R. Wasielewski, *J. Phys. Chem. B* 2013, **117**, 2195.

Graphical Abstract

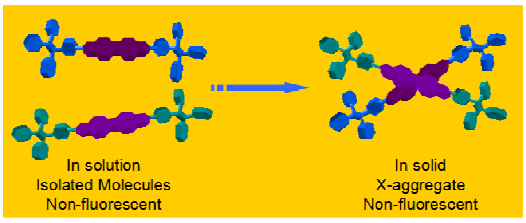

Perylene-bisimides (PBIs) modified with tetraphenylethene (TPE) at N-terms show unique X-aggregation and are non-fluorescent in solution, aggregate and solid film due to the photoinduced charge transfer between TPE and PBI subunits.